# V.D.2 Nanostructured Metal Carbide Catalysts for the Hydrogen Economy

Ram Seshadri (Primary Contact)[1,2], Susannah Scott[3,4], Juergen Eckert[2]
Post docs and students: Dr. Jun Li[2], Robert Savinelli[4], Katharine Page[1,2]
Affiliations: [1]Materials Department, [2]Materials Research Laboratory, [3]Chemical Engineering, and [4]Chemistry
University of California
Santa Barbara, CA 93106.
Phone: (805) 893-6129; Fax: (805) 893 8797
E-mail: seshadri@mrl.ucsb.edu

Program Officer: Raul Miranda
Phone: (301) 903-8014
E-mail: Raul.Miranda@science.doe.gov

## Objectives

Our goal is to develop preparative routes to nanostructured transition metal (Mo and W) carbides with high surface area and desired bulk and surface structures as catalysts for $H_2$ generation. We will examine the catalytic behavior of these novel carbides for fuel reforming and water-gas shift and initiate fundamental understanding of the surface chemistry in $H_2$ generation catalysis. We will explore the nature of the active sites through a combination of advanced *in situ* spectroscopic techniques and density functional calculations interfaced directly with the experiment.

## Technical Barriers

The greatest impediment to the widespread application of metal carbides as catalysts seems to be their materials science, rather than their reactivity. The challenge is to prepare stable, high surface area forms of specific phases or, at least, to ensure that the exposed surfaces have the correct structure. Existing strategies of making high surface area carbides generally produce nonstoichiometric surfaces, containing either residual oxygen or excess carbon which can block the active surface. Amongst the goals of our research is to utilize modern techniques of structure analysis such as neutron pair-distribution function analysis to aid in our understanding of these fascinating catalytic materials.

## Abstract

Nanostructured, high-porosity molybdenum and tungsten carbides were prepared by thermal decomposition and carburization of ammonium paramolybdate $(NH_4)_6Mo_7O_{24}.4H_2O$ and ammonium paratungstate $(NH_4)_{10}W_{10}O_{41}$ in flowing 50%$CH_4$/ 50%$H_2$. The structures were investigated by X-ray and neutron diffraction, and the presence of amorphous carbon was studied by neutron diffraction and neutron pair distribution function analysis. XPS analysis on the exposed surface shows that the oxidation states of the metals are almost exclusively Mo(II) and W(IV), and the amount of carbidic carbon is much higher in $Mo_2C$ than in WC. BET surface areas of $Mo_2C$ and WC were found to be as high as 68 $m^2/g$ and 21 $m^2/g$, respectively, and these *do not* arise from the amorphous carbon on the surface. Pore size distribution revealed the existence of unique combined micro- and meso-porosity at a range of 2 to 30 nm, and a strong correlation between specific surface area and the pore volume. Electron microscopy provided further evidence for the formation of the nanopores in as-prepared carbides. For the first time, EXAFS analyses have been carried out beyond the first coordination shells of these materials, and good agreement has been achieved between the data and the fit based on structural models derived from neutron diffraction refinement.

## Progress Report

### Characterization by Diffraction, Neutron PDF and XPS

As-prepared Mo and W carbide samples were analyzed by X-ray and neutron powder diffractions, neutron pair distribution function (PDF) calculation, and X-ray photoelectron spectroscopy (XPS). XRD patterns of the samples were obtained using Philips XPERT X-ray diffractometer with Cu $K\alpha$ radiation. Neutron powder diffraction data were collected on the BT-1 32-counter high resolution diffractometer at the NIST Center for Neutron Research. X-ray diffraction data of $Mo_2C$ can be fitted almost equally well to either hexagonal ($P6_3/mmc$) or orthorhombic ($Pbcn$) structure model, but extra peaks arise from orthorhombic symmetry in neutron diffraction pattern. The crystal structure of $Mo_2C$ was therefore refined in orthorhombic space group *Pbcn* [1], and WC in hexagonal space group *P*-6*m*2 [2] using Fullprof software. The Rietveld refinement results on neutron data are shown in Figure 1. The mismatch between the observed and the calculated data is presumably due to stacking faults, especially in WC [3].

Non-carbidic or amorphous carbon can not be detected by X-ray diffraction. Neutron diffraction pattern of WC, however, clearly shows an additional phase attributed to graphite carbon (Figure 1). This is in agreement with the neutron pair distribution function

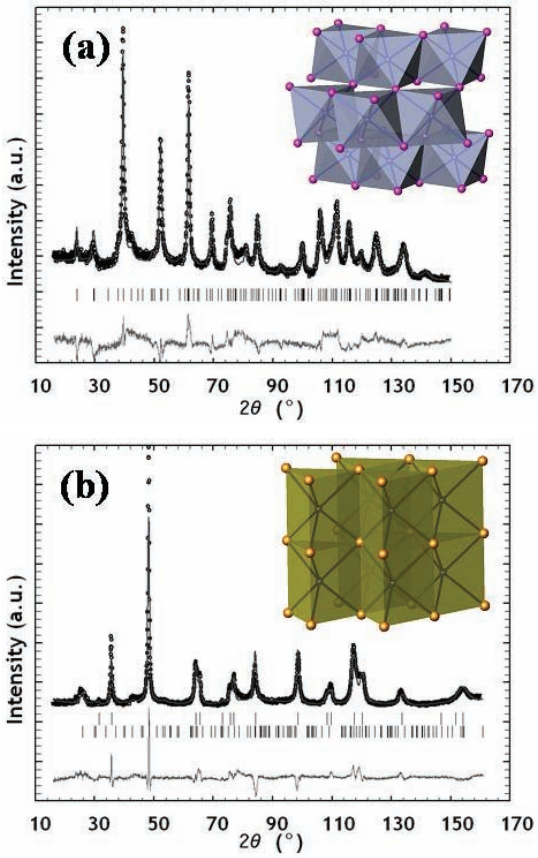


**FIGURE 1.** Observed (circles) and calculated (gray line) neutron diffraction patterns for $Mo_2C$ (a) and WC (b). Vertical bars indicate allowed peak positions for each phase. Bottom curve is the difference pattern. The insets are the crystal structures with Mo in purple, W in orange and C in blue in the center of the polyhedra (a,b).

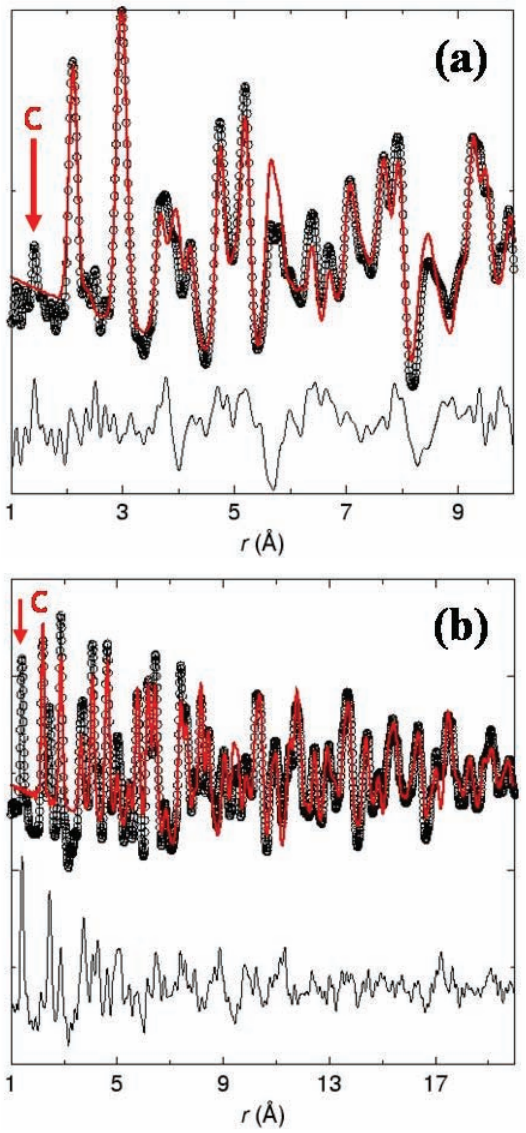


**FIGURE 2.** Neutron pair distribution function (PDF) analysis on non-carbidic carbon in (a) $Mo_2C$ and (b) WC samples. The difference between observed (black circles) and calculated (red lines) data is shown as black curves in the bottom.

analysis of neutron total scattering data. (Figure 2). In Figure 2, calculated patterns are fitted to the crystal structure of carbides, and the difference curves can be fitted to the graphite structure. The most intense peaks assigned to graphite carbon are marked with arrows.

The contribution from the graphite phase is much larger in WC than in $Mo_2C$, indicating a higher amount of non-carbidic carbon in WC which is likely caused by the higher carburization temperature. Neutron diffraction and scattering data for PDF analysis were collected on NPDF at the Lujan Center at Los Alamos Neutron Center.

Surface compositions and metal oxidation states were measured by X-ray photoelectron spectroscopy using a Kratos Axis Ultra spectrometer with an Al Kα source. The carbon 1*s* peak at 284.8 eV was used as a reference for binding energy calibration.

This peak (Figure 3 (a),(b), purple) is assigned to background adventitious carbon presumably from vacuum pump oil as well as amorphous carbon from the sample surface. It is therefore hard to determine the amount of surface amorphous carbon and metal to carbon ratio. Despite all that, the relative amount of carbidic carbon (283.5 eV) [4] is much higher in $Mo_2C$ than in WC (Figure 3 (a),(b), blue), possibly because the surface of WC is covered with more amorphous carbon and therefore less carbidic carbon is exposed. Spectra in Mo 3*d* and W 4*f* regions (Figure 3 (c),(d)) show the expected doublets with chemical shifts characteristic of Mo(II) and W(IV), corresponding to the desired $Mo_2C$ and WC forms. The presence of some higher oxidation states is due to partial oxidation of the surface.

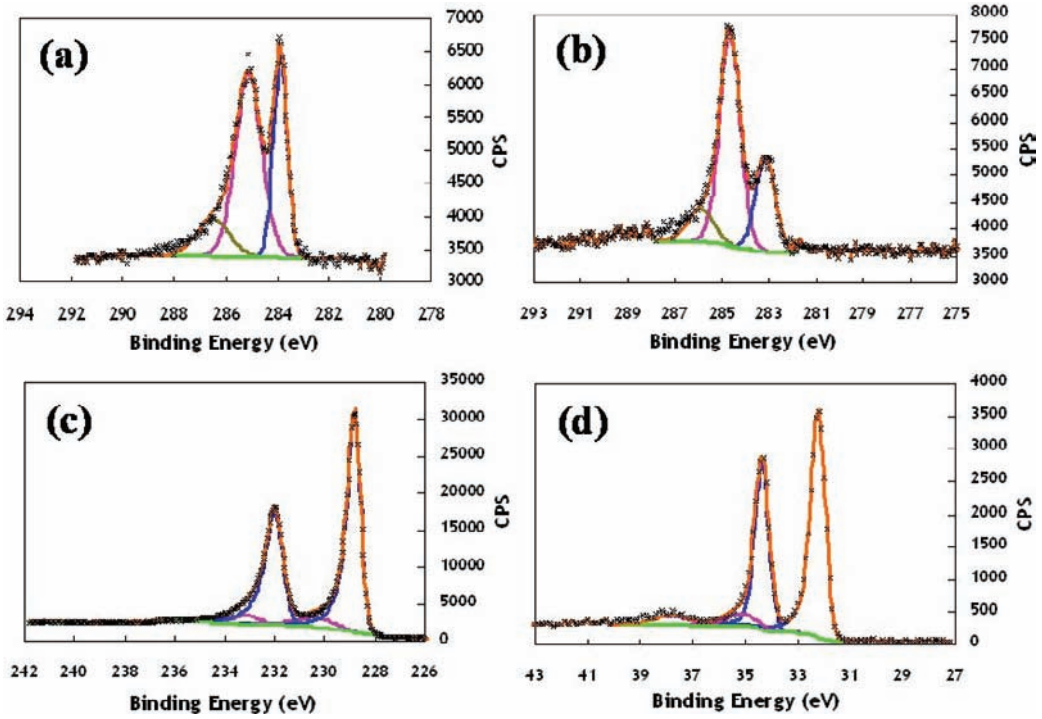


**FIGURE 3.** High resolution XPS spectra (black) on (a) $Mo_2C$ and (b) WC in C 1*s* region, (c) $Mo_2C$ in Mo 3*d* region, (d) WC in W 4*f* region. Fits to the data are in orange and background in green.

### Characterization by $N_2$ Sorption and Electron Microscopy

The BET surface areas were determined on a Micromeritics TriStar 3000 sorption analyzer by low temperature $N_2$ absorption method.

Pore size distributions (Figure 4) were derived from the adsorption branch of the isotherms using BJH model. Higher surface area is related with larger pore volume. Micro- and meso-pores in the range of 2 to 30 nm were observed, which is consistent with the electron microscopy analysis (Figure 5 and Figure 6).

Secondary electron field emission scanning electron microscopy (SEM) was performed on a Sirion XL30 microscope. High resolution transmission electron microscopy (HRTEM) and Z-contrast images were obtained from a FEI Tecnai F30UT transmission electron microscope equipped with a field-emission electron gun operated at 300 kV. In scanning TEM (STEM) mode, atomic number sensitive high-angle annular dark-field (HAADF) images were recorded using an annular dark field detector in combined with an electron dispersive X-ray detector (EDAX-R, 135eV) for chemical analysis. EDX line scan profile shows the expected distribution of molybdenum across the nanopores (Figure 6). The porous morphologies are very promising for catalysis.

### Characterization by X-ray Absorption Fine Structure

Mo K-edge (20,000 eV) and W L3-edge (10,207 eV) XAS spectra were collected in unfocused mode using Si(220) $\phi = 0$ crystals on beamline 2-3 at the Stanford Synchrotron Radiation Laboratory (SSRL).

EXAFS refinement adopts the structure models derived from the Rietveld refinement of neutron powder diffraction data. Good agreement between the data and the fit has been achieved in the range 1 to 5 Å, nearly twice the range found in ref.[5].

## Future Directions

We have determined methods of making stable high-surface area nanostructured molybdenum and tungsten carbides, we are in a position to carefully establish the relation between the degree of crystallinity and structural coherence, and the catalytic activity. We will focus on methods controlling and removing the surface graphite, and aim for sill higher surface area. We will continue to establish methods for suppressing amorphous carbon deposition on the surface, and verify that the porous morphology is retained after being subject to catalytic conditions. We will also seek new preparative strategies such as ethanolic precipitation [8] of the Mo and W

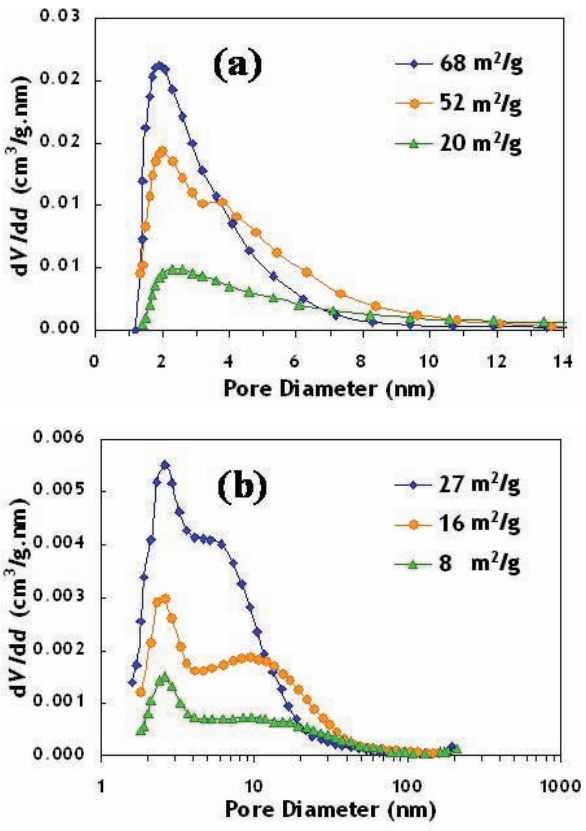


**FIGURE 4.** Pore size distributions of (a) $Mo_2C$ and (b) WC samples with different surface areas.

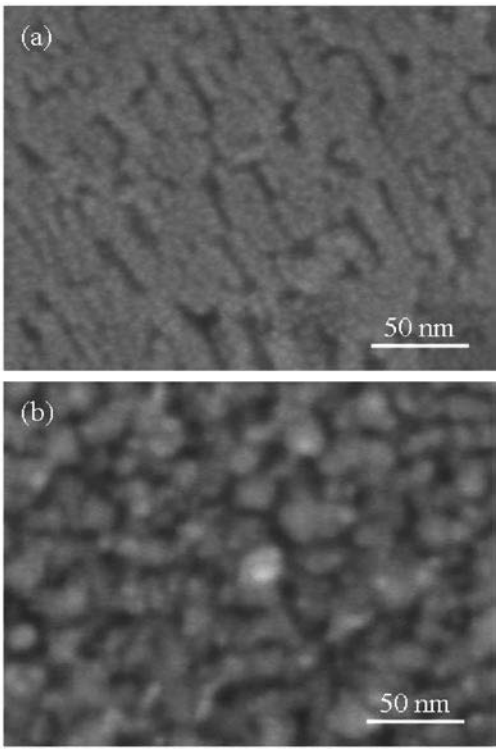


**FIGURE 5.** Nanostructured $Mo_2C$ (a) and WC (b) revealed by SEM.

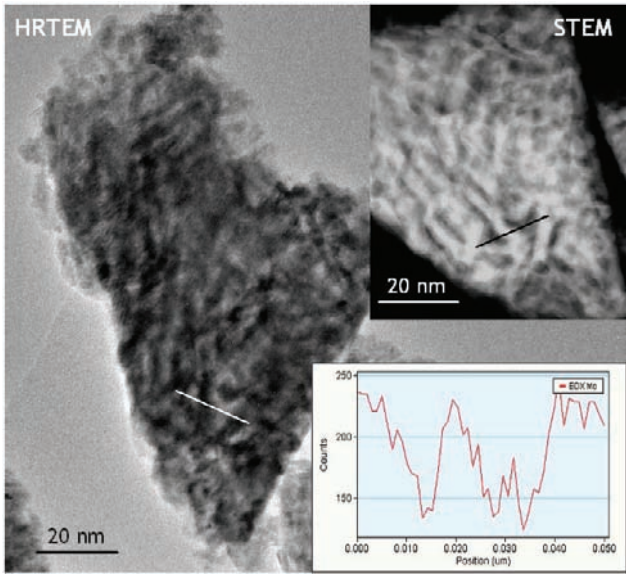


**FIGURE 6.** Nanoporous $Mo_2C$. The inset in bottom right corner displays EDX line scan for elemental molybdenum along the marked lines in the left HRTEM and top STEM images.

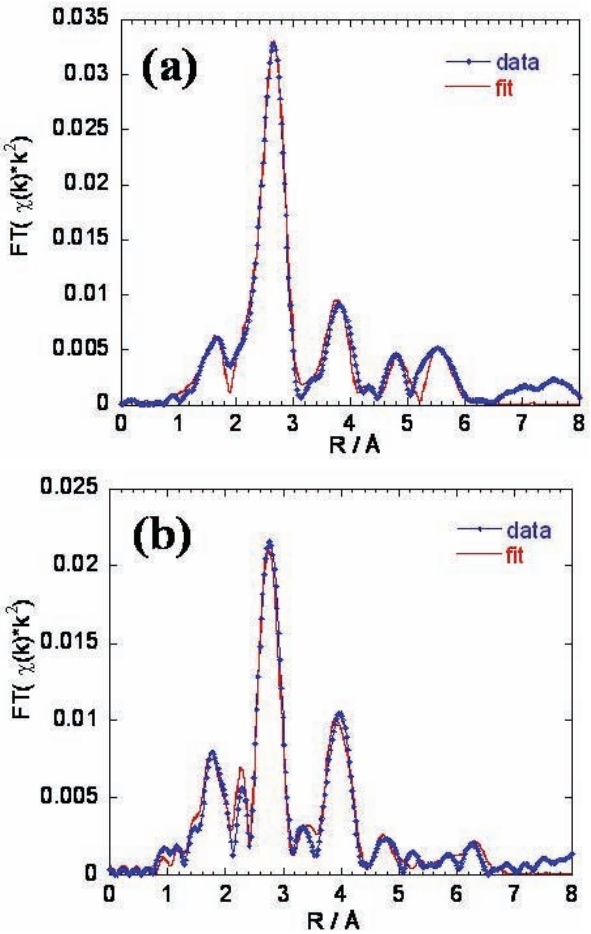


**FIGURE 7.** Mo K-edge (a) and W L3-edge (b) EXAFS (blue) in R-space for $Mo_2C$ and WC samples, showing fit (red) to $Mo_2C$ and WC crystal structures.

precursors in the presence of supporting oxides such as $Al_2O_3$ to make supported carbides with larger active surfaces.

## References

**1.** T. Epicier, J. Dubois, C. Esnouf, and G. Fantozzi, *Acta Metall*. **36** (1988) 1891–1901.

**2.** J. Leciejewicz, *Acta Crysallogr.* **14** (1961) 200–201.

**3.** M. K. Hibbs, and R. Sinclair, *Acta Metall*. **29** (1981) 1645–1654.

**4.** T. P. St. Clair, S. T. Oyama, and D. F. Cox, *Surf. Sci*. **468** (2000) 62–76.

**5.** W. Ding, S. Li, G. D. Meitzner, and E. Iglesia, *J. Phys. Chem. B* **105** (2001) 506–513.

**6.** A. K. Cheetham, *Nature* **288** (1980) 469–470.

## Publications and Acknowledgements

**1.** J. Li, K. Page, R. Savinelli, H. Szumila, J. P. Zhang, S. L. Scott and R. Seshadri. *An investigation of the structure and surface of nanoporous $Mo_2C$ and WC.* 2007, in preparation.

**2.** R. Savinelli, J. Li, R. Seshadri, and S. L. Scott. *X-ray photoelectron and absorption spectroscopy study of nanoporous $Mo_2C$ and WC.* 2007, in preparation.

This work has been supported by the Department of Energy (DOE) Office of Basic Energy Sciences (BES) through grant DE-FG02-05ER15025. The work at UCSB made use of facilities of the Materials Research Laboratory, supported by the NSF (DMR05-20415). We acknowledge the support of the National Institute of Standards and Technology, U.S. Department of Commerce, the Los Alamos Neutron Science Center, funded by DOE office of BES, in providing the neutron research facilities, and Stanford Synchrotron Radiation Laboratory (SSRL).